Published in final edited form as:
Biochemistry. 2013 January 8; 52(1): 125–131. doi:10.1021/bi301099k.

Water Networks in Fast Proton Transfer During Catalysis by Human Carbonic Anhydrase II[†]

Rose Mikulski[a], **Dayne West**[b], **Katherine H. Sippel**[b], **Balendu Sankara Avvaru**[b], **Mayank Aggarwal**[b], **Chingkuang Tu**[a], **Robert McKenna**[*,b], and **David N. Silverman**[*,a,b]

[a] Department of Pharmacology, University of Florida, Gainesville, FL 32610, USA

[b] Department of Biochemistry and Molecular Biology, University of Florida, Gainesville, FL 32610, USA

Abstract

Variants of human carbonic anhydrase II (HCA II) with amino-acid replacements at residues in contact with water molecules in the active-site cavity have provided insights into the proton transfer rates in this protein environment. X-ray crystallography and ^{18}O exchange measured by membrane inlet mass spectrometry have been used to investigate structural and catalytic properties of variants of HCA II containing the replacements of Tyr7 with Phe (Y7F) and Asn67 with Gln (N67Q). The rate constants for proton transfer from His64 to the zinc-bound hydroxide in catalysis were 4 μs^{-1} and 9 μs^{-1} for Y7F and Y7F-N67Q, respectively, compared with a value of 0.8 μs^{-1} for wild-type HCA II. These higher values observed for Y7F and Y7F-N67Q HCA II could not be explained by differences in the values of the pK_a of the proton donor (His64) and acceptor (zinc-bound hydroxide) or by orientation of the side chain of the proton shuttle residue His64. They appeared to be associated with reduced branching in the networks of hydrogen-bonded water molecules between the proton shuttle residue His64 and the zinc-bound solvent molecule as observed in crystal structures at 1.5 – 1.6 Å resolution. Moreover, Y7F-N67Q HCA II is unique among the variants studied in having a direct, hydrogen-bonded chain of water molecules between the zinc-bound solvent and N^{δ} of His64. This study provides the clearest example to date of the relevance of ordered water structure to rate constants for proton transfer in catalysis by carbonic anhydrase.

The carbonic anhydrases (CAs) are primarily zinc metalloenzymes that rapidly hydrate carbon dioxide to form bicarbonate and a proton. The well studied α class includes the mammalian CAs with roles in acid-base balance, fluid secretion, respiration, and other physiological processes (1). Humans are known to express many CA isozymes throughout the body (1, 2), including the structurally and kinetically well characterized human carbonic anhydrase II (HCA II) (3-5). The first stage of the catalysis is the binding of bicarbonate to zinc followed by the dehydration of bicarbonate (eq 1). The second stage is the transfer of a proton from buffer in solvent BH^+ to the proton shuttle His64 and subsequently to zinc-bound hydroxide to regenerate the catalytic zinc-bound water (eq 2).

[†]This work was supported by a grant from the National Institutes of Health GM25154.

[*]Corresponding authors: D.N.S. Department of Pharmacology, College of Medicine, University of Florida, Box 100267, Gainesville, Florida 32610; Phone: (352) 392 3556; Fax (352) 392 9696; silvrmn@ufl.edu; R.M. Department of Biochemistry and Molecular Biology, College of Medicine, University of Florida, Box 100245, Gainesville, Florida 32610; Phone: 352-392-5696; Fax: 352-392-3422; rmckenna@ufl.edu..

Supporting Information Available

Supporting information consists of a table of steady-state constants for the hydration of CO_2 and dehydration of bicarbonate catalyzed by wild-type and Y7F-N67Q HCA II, and a double mutant cycle for the values of k_B for catalysis by the enzymes of Table 2. This material is available free of charge via the Internet at http://pubs.acs.org.

$$EZnH_2O+HCO_3^- \overset{-H_2O}{\rightleftarrows} EZnHCO_3^- \rightleftarrows EZnOH^-+CO_2 \quad (1)$$

$$His64-EZnOH^-+BH^+ \rightleftarrows H^+His64-EZnOH^-+B \rightleftarrows His64-EZnH_2O+B \quad (2)$$

The intramolecular proton transfer from His64 to the zinc-bound hydroxide in the second stage of the catalysis (eq 2) is as fast as 1 μs^{-1} and is rate limiting for the maximal velocity of HCA II (6, 7). The position of the side-chain of His64 is observed in inward and outward orientations (Figure 1); in the inward orientation the imidazole ring of His64 is about 7.5 Å from the zinc (8-10). An ordered, hydrogen-bonded network of water molecules extending between the zinc-bond water and His64 is observed in crystal structures of HCA II (Figure 1) and is believed to offer clues to the pathway for intramolecular proton transfer in catalysis (3-5).

The water network in HCA II appears to form hydrogen bonds with hydrophilic residues lining the active-site cavity and is branched at the water molecule labeled W2 in Figure 1. A number of studies have replaced residues in the active-site cavity altering the structure of the water network as well as changes in the orientation of His64 and the pK_a of its imidazole ring (11-13) in order to determine the relevance of the observed water structure to the rate constants for proton transfer. One significant observation is that the variant of HCA II with Tyr7 replaced with Phe (Y7F) has an enhanced rate constant of intramolecular proton transfer, five-fold greater than wild type, and less branching of the water network connecting His64 and the zinc-bound solvent (11). Computational studies indicate that the rate of proton transfer is expected to be faster in unbranched water chains (14, 15).

In this work we have constructed the variant Y7F-N67Q HCA II that has a water network showing less branching than in wild type. It also has a completed hydrogen-bonded water chain and a shorter distance between His64 and the zinc-bound solvent as determined from the crystal structure at 1.6 Å resolution. The appropriate single mutants Y7F and N67Q HCA II are also examined. For the double mutant the rate constant for intramolecular proton transfer at 9.0 μs^{-1} is ten-fold greater than wild type measured by ^{18}O exchange. This allows a more complete understanding of the factors that influence proton transfer through water chains in a protein environment. HCA II serves as a simple model for examining proton transfers in more complex systems such as the photosynthetic reaction center, bacteriorhodopsin, and cytochrome c oxidase.

METHODS

Enzymes

Variants of HCA II were made with the QuickChange II Site-Directed Mutagenesis Kit (Agilent) on the expression vector coding the full-length wild-type HCA II. The entire region coding HCA II was determined for each mutant to confirm the correct DNA sequence. Plasmids were transformed for expression into *Escherichia coli* BL21(DE3)pLysS cells (Agilent). The transformed cells were grown in LB media to which was added 1.0 mM $ZnSO_4$ and induced with 1.0 mM IPTG when the $OD_{600\ nm}$ reached 0.6. Each variant was purified by affinity chromatography using p-(aminomethyl)benezene-sulfonamide coupled to agarose beads (Sigma)(16). The concentration of HCA II and variants was determined by titration of active sites by the tight-binding inhibitor ethoxzolamide while measuring activity by the ^{18}O method.

Oxygen-18 exchange

The catalysis of HCA II has been well studied by measuring the exchange of ^{18}O from labeled bicarbonate and CO_2 species to water using membrane inlet mass spectrometry (17). The method is based on the depletion of ^{18}O from CO_2 that passes across the membrane inlet into a mass spectrometer (Extrel EXM-200). The apparatus allows a continuous measurement of isotopic content of CO_2 under controlled conditions in solution. The initial step of the catalysis by HCA II is the dehydration of labeled bicarbonate with a probability of leaving a ^{18}O-labeled hydroxide at the zinc (eq 3). The second step involves the protonation of the zinc-bound hydroxide subsequently releasing $H_2{}^{18}O$ which is very greatly diluted by $H_2{}^{16}O$ in solution (eq 4).

$$HCOO^{18}O^{-}+EZnH_2O \rightleftarrows EZnHCOO^{18}O^{-} \rightleftarrows COO+EZn^{18}OH^{-} \quad (3)$$

$$H+His64-EZn^{18}OH^{-} \overset{H_2O}{\rightleftarrows} His64-EZnH_2{}^{18}O \rightarrow His64-EZnH_2O+H_2{}^{18}O \quad (4)$$

The ^{18}O-exchange method allows a rate for both steps of the catalysis to be determined (17). The rate of the first step, exchange between CO_2 and HCO_3^- at chemical equilibrium, is designated R_1 and described by eq 5. The maximal rate constant of the conversion between CO_2 and HCO_3^- is k_{cat}^{ex}, the apparent binding constant of the substrate to enzyme is K_{eff}^{S}, and [S] is the concentration of the substrate either CO_2 or bicarbonate for the hydration or dehydration direction (18). The ratio k_{cat}^{ex}/K_{eff}^{S} is in principle and practice equivalent to k_{cat}/K_m determined in steady state experiments (18).

$$R_1/[E] = k_{cat}^{ex}CO_2/\left(K_{eff}^{CO2}+CO_2\right) \quad (5)$$

The rate of the second step, the transfer of a proton and release of water in eq 4, is termed R_{H2O}. The R_{H2O} is interpreted in terms of a rate constant k_B for proton transfer to the zinc-bound hydroxide (eq 6). The ionization constants of the proton donor and the zinc-bound water molecule are given in eq 6 as $(K_a)_{donor}$, and $(K_a)_{ZnH2O}$.

$$R_{H2O}/[E] = k_B/\left(\left[1+(K_a)_{donor}/[H^+]\right]\left[1+[H^+]/(K_a)_{ZnH2O}\right]\right) \quad (6)$$

The uncatalyzed and carbonic anhydrase catalyzed ^{18}O exchange at chemical equilibrium was measured in the absence of buffer at a total substrate concentration (all CO_2 species) of 25 mM using membrane-inlet mass spectrometry (17). Reactions were carried out at 10 °C and 25 °C as noted, and total ionic strength of solution was maintained at 0.2 M by the addition of Na_2SO_4. The determination of the kinetic and ionization constants of eqs 5 and 6 were carried out by nonlinear least-squares methods (Enzfitter, Biosoft).

Crystallography

Crystals of the mutants N67Q and Y7F-N67Q HCA II were obtained using the hanging drop method (19). The crystallization drops were prepared by mixing 5 μL of protein [concentration ~15 mg/mL in 100 mM Tris-HCl (pH 8.0)] with 5 μL of the precipitant solution [1.25 M sodium citrate, 100 mM Tris-Cl (pH 8.0)] against a well of 1000 μL precipitant solution. Crystals were observed within a week at 293K.

The N67Q and Y7F-N67Q HCAII crystals were flash cooled after a soak in cryo-protectant, 30% glycerol plus precipitant solution, before mounting. The x-ray data were obtained at 100K using an R-AXIS V++ optic system from Viarimax HR a Rigaku RU-H3R Cu rotating

anode operating at 50 kV and 100 mA. The detector to crystal distance was set to 80 mm. The oscillation steps were 1° with a 6 min exposure per image for 360 degrees. Data set statistics for the crystals are given in Table 1.

The model building was done manually with the program Coot (20) and refinement was carried out with PHENIX suite (21). The starting phasing model was the wild-type HCA II structure of Fisher *et al.* (22) (PDB code: 1tbt) with the waters removed and the mutated residues as well as His64 changed to Ala to reduce model bias.

RESULTS

Catalysis

The pH dependence of catalysis of the hydration of CO_2 determined by ^{18}O exchange was determined for each of the variants Y7F, N67Q, and Y7F-N67Q HCA II. The data for Y7F HCA II were reported previously (11). Profiles of R_1/[E] over a range of pH were obtained, and eq 5 was used to determine the catalytic constants $k_{cat}^{ex}/K_{eff}^{CO2}$ for hydration of CO_2 (Figure 2). Ionic strength was maintained at 0.2 M using Na_2SO_4 and the substrate was $NaHCO_3$; pH was adjusted with dilute H_2SO_4 and no buffers were added. Fits to a single ionization appear satisfactory except at very low pH < 6 where the data showed decreased values for $k_{cat}^{ex}/K_{eff}^{CO2}$ possibly due to additional ionizations or denaturation. This was particularly apparent in the variants containing the replacement Y7F, as already noted for Y7F HCA II (11). The maximal pH independent values of $k_{cat}^{ex}/K_{eff}^{CO2}$ are compared in Table 2; these are similar with values between 50 and 120 $\mu M^{-1}s^{-1}$. The pK_a values of the zinc-bound water, pK_{aZnH2O}, determined from the fits to a single ionization obtained from the pH profiles of $k_{cat}^{ex}/K_{eff}^{CO2}$ (Table 3, column 2) are also quite similar. These similarities reflect the distances of these residues from the zinc: 7.0 Å between the hydroxyl oxygen of Tyr7 and the zinc, and 8.4 Å between the carboxamide carbon of Asn67 and the zinc.

The advantage of the ^{18}O exchange method is that catalysis by variants of CA can be examined in solutions without added buffer to determine rates of intermolecular proton transfer. Experiments carried out at steady state do not have this advantage and must use external buffers to control pH. The rate constant R_{H2O}/[E] measures the second stage of catalysis in which rate-limiting intermolecular proton transfer releases $H_2{}^{18}O$ from the active site (eq 4). The pH profiles of R_{H2O}/[E] for each mutant were predominantly bell-shaped (Figure 3), reflecting the proton transfer from the imidazolium side chain of His64 to the zinc-bound hydroxide (23). The bell-shaped curves were fit to eq 6 to yield a rate constant of proton transfer k_B. The range in values of k_B was approximately ten-fold (Table 2). Since the values of pK_a were nearly identical for the proton donor (His64) and acceptor, there was no issue in assignment of these values. The exception is Y7F HCA II in which the pK_a of the zinc-bound water was confirmed by measurement of the esterase activity (11).

Crystallography

The crystal structures of the variants N67Q and Y7F-N67Q of HCAII were solved to 1.5-1.6Å resolution using data that had completeness greater than 92% (Figures 4, 5). Figure S1 (Supporting information) shows the omit maps with electron densities. The crystal structure data and refinement statistics are listed in Table 1. Overall, no major structural perturbations were observed; the RMSD for C^{α} atoms was 0.1 Å for both variants when compared to the wild-type HCA II (PDB code 2ili (8)). The proton shuttle residue His64 has been shown to occupy two conformations in wild-type HCA II, inward and outward with respect to orientation in the active-site cavity (8, 10). The outward conformation was dominant in N67Q HCA II while the inward conformation was observed in Y7F-N67Q

HCA II, similar to the Y7F variant previously published (11). Coordinates for N67Q HCA II and Y7F-N67Q HCA II have been deposited in the Protein Data Bank with code numbers 3TVN and 3TVO, respectively.

Compared with wild-type HCA II, the hydrogen-bonded solvent network in the active site cavity was mostly conserved for the three variants of HCA II depicted in Figures 1, 4 and 5. However, there were distinct differences. In the case of Y7F, the water molecule labeled W3A was not observed (Figure 5 (11)). For Y7F-N67Q HCA II, W3A was observed but was not within hydrogen bonding distance to W2; moreover, the distance between W3B and W2 (3.1 Å) was longer than in wild type (2.7 Å)(Table 4). In addition, in Y7F-N67Q the distance between W2 and N^{δ} of His64 (2.8 Å) is shorter, and hence indicates a stronger hydrogen bond than in wild type for which His64 is inward (3.2 Å) (Table 4). This is also reflected in the respective distances between the zinc-bound solvent and N^{δ} of His64 (Table 4). The carboxamide group of the Gln substitution at residue 67 extended further into the active site cavity than the Asn residue it replaced. For N67Q, an associated effect was an increase in the distance from the zinc-bound solvent to the N^{δ} of His64 (10.5 Å, outward orientation) compared with wild type (10.0 Å, outward, Table 4).

DISCUSSION

These catalytic and structural results on variants of HCA II with amino-acid replacements at residues in contact with water molecules in the active-site cavity provide insight into the proton transfer rates in this protein environment. The rate constant k_B of 9 μs^{-1} for proton transfer from His64 to the zinc-bound hydroxide in catalysis by N67Q-Y7F HCA II (Table 2) is the fastest measured for a variant of this isozyme. The previously studied Y7F HCA II was also found to have rapid proton transfer at k_B of 4 μs^{-1} (11). The value for wild-type HCA II is k_B = 0.8 μs^{-1} (Table 2)(11).

These high k_B values observed for Y7F and Y7F-N67Q HCA II were not explained by differences in the values of the pK_a between the proton donor (His64) and acceptor (zinc-bound hydroxide). This is shown in Table 3 in which the values of pK_a are similar for these variants. Moreover, previous reports showed that the pH dependence of k_B is rather flat in the vicinity of ΔpK_a ($pK_{aZnH2O} - pK_{a\ His64}$) near zero (24, 25). We can comment, however, that the increments in the rate constant for proton transfer k_B caused by the replacements at residues 7 and 67 are additive in nature, as illustrated in a double mutant cycle (Scheme S1, Supporting Information)(26).

In the cases of Y7F and N67Q-Y7F HCA II, the enhanced rate constants are associated with a predominant inward orientation of the His64 side chain in the crystal structures (Figure 5). However, the orientation of His64 in crystal structures has not been shown to affect the rate constant for proton transfer according to the following data. The variant N62L has His64 predominantly inward and N67L predominantly outward with other aspects of their protein structure nearly identical, yet their values of k_B are the same at 0.2 μs^{-1} (11, 12, 27). The same conclusion that the inward and outward conformations in crystal structures of His64 do not influence the proton transfer rate was reached using a mutant with the substitution of Thr200 with Ser (28). This is supported by computational studies which suggest that the orientation of His64 need not influence this intramolecular proton transfer rate (29, 30).

It remains then to examine the solvent structure observed in the active site. Although these low energy networks of ordered water are observed in crystal structures and are taken as significant clues of the proton transfer pathway, clusters of hydrogen bonded water in the active-site cavity in solution have lifetimes typically in the picosecond range (31). Comparison of the crystal structures of the variants of Table 2 and other reports of variants

of HCA II (11, 12, 32) shows that the two most efficient enzymes in proton transfer Y7F and Y7F-N67Q HCA II have less branched water structure, specifically water molecule W3A is not observed in Y7F and is not within hydrogen bond distance of the water chain in Y7F-N67Q (Figure 5; Table 4). Furthermore, in Y7F-N67Q there is a long and weak hydrogen bond between W2 and W3B compared with wild type (Figure 5, Table 4). We also point out that this double mutant is unique among the variants of HCA II we have examined in that it shows a normal hydrogen bond length between W2 and the N^{δ} of His64, other variants show this as a very weak hydrogen bond at best (Table 4). Thus, Y7F-N67Q has the most completely formed hydrogen-bonded chain of unbranched water molecules between the zinc-bound solvent and N^{δ} of His64 among the variants examined (Table 4). Computations show that proton transfer through an unbranched, hydrogen-bonded water network is more rapid than through a branched pathway (14, 15, 33). This feature of a more direct pathway in the structures of Y7F and Y7F-N67Q HCA II appears to be most relevant in explaining the proton transfer efficiencies of these variants.

When catalysis was measured by stopped-flow spectrophotometry, the steady-state constants k_{cat} for dehydration were close in magnitude for wild type (0.24 μs^{-1}) and Y7F-N67Q (0.19 μs^{-1}), as were the values of k_{cat} for hydration (Table S1, Supporting Information). The steady-state constant k_{cat} measures many steps in either the dehydration or hydration directions, among which are conversion of bound substrate to product, product dissociation, intramolecular proton transfer, and possibly proton transfer steps between buffer in solution and zinc-bound hydroxide via His64. At steady-state, enzyme species are not necessarily at equilibrium concentrations, and the enzyme species preceding a rate-limiting step accumulates above equilibrium concentrations. The solvent H/D kinetic isotope effects on k_{cat} for hydration of CO_2 catalyzed by wild-type and Y7F-N67Q CA II are near 3.2 for both enzymes measured in the presence of excess buffer (Table S1). This indicates that proton transfer is a predominant rate-contributing step for both the wild type and variant measured at steady state.

The ^{18}O exchange rate for proton transfer R_{H2O} from which we obtain k_B is determined at chemical equilibrium and focuses more on proton transfer because it contains many fewer steps of the catalysis than k_{cat}. In the ^{18}O exchange experiment there is no buffer in solution, and since there is relatively little proton transfer between the enzyme and solution there is no need for His64 to change orientation to sustain catalysis. These features provide an explanation why k_B is greater than k_{cat}. The results are consistent with the influence of the structure of the specific water chains through which proton transfer occurs. In view of the many potential proton transfer pathways that have been found in CA II (34), the data reflect the different proton transfer pathways involved in the equilibrium and steady-state experiments that result in different rate constants.

This study with the greatly enhanced proton transfer of Y7F-N67Q HCA II provides the clearest example to date of the relevance of the ordered water structure to rate constants for proton transfer in catalysis by carbonic anhydrase. The complement of these studies with the pertinent computational results of rapid proton transfer through unbranched water chains (14, 15, 31) is gratifying. It appears that the arrays of ordered, hydrogen-bonded water molecules as observed in crystal structures provide relevant information to explain efficient intramolecular proton transfer in carbonic anhydrase.

Supplementary Material

Refer to Web version on PubMed Central for supplementary material.

ABBREVIATIONS

N67Q HCA II	the variant of human carbonic anhydrase II containing the replacement of Asn67 by Gln
AE	anion exchange protein
PDB	Protein Data Bank
RMSD	root mean squared deviation

REFERENCES

1. Chegwidden, WR.; Carter, ND.; Edwards, YH. The Carbonic Anhydrases New Horizons. Birkhauser Verlag; Basel: 2000.
2. Supuran, CT.; Scozzafava, A.; Conway, J. Carbonic Anhydrase - Its Inhibitors and Activators. CRC Press; Boca Raton: 2004.
3. Silverman DN, McKenna R. Solvent-Mediated Proton Transfer in Catalysis by Carbonic Anhydrase. Acc Chem Res. 2007; 40:669–675. [PubMed: 17550224]
4. Christianson DW, Fierke CA. Carbonic anhydrase: Evolution of the zinc binding site by nature and by design. Accounts of Chemical Research. 1996; 29:331–339.
5. Lindskog S. Structure and mechanism of carbonic anhydrase. Pharmacol Ther. 1997; 74:1–20. [PubMed: 9336012]
6. Khalifah RG. Carbon Dioxide Hydration Activity of Carbonic Anhydrase.1. Stop-Flow Kinetic Studies on Native Human Isoenzyme-B and Isoenzyme-C. Journal of Biological Chemistry. 1971; 246:2561–2573. [PubMed: 4994926]
7. Steiner H, Jonsson BH, Lindskog S. Catalytic Mechanism of Carbonic-Anhydrase - Hydrogen-Isotope Effects on Kinetic-Parameters of Human C Isoenzyme. European Journal of Biochemistry. 1975; 59:253–259. [PubMed: 1249]
8. Fisher SZ, Maupin CM, Budayova-Spano M, Govindasamy L, Tu C, Agbandje-McKenna M, Silverman DN, Voth GA, McKenna R. Atomic crystal and molecular dynamics simulation structures of human carbonic anhydrase II: Insights into the proton transfer mechanism. Biochemistry. 2007; 46:2930–2937. [PubMed: 17319692]
9. Liljas A, Lovgren S, Bergsten PC, Carlbom U, Petef M, Waara I, Strandbe B, Fridborg K, Jarup L, Kannan KK. Crystal-Structure of Human Carbonic Anhydrase-C. Nature-New Biology. 1972; 235:131–137. [PubMed: 4621826]
10. Nair SK, Christianson DW. Unexpected pH-Dependent Conformation of His-64, the Proton Shuttle of Carbonic Anhydrase-II. Journal of the American Chemical Society. 1991; 113:9455–9458.
11. Fisher SZ, Tu CK, Bhatt D, Govindasamy L, Agbandje-McKenna M, McKenna R, Silverman DN. Speeding up proton transfer in a fast enzyme: kinetic and crystallographic studies on the effect of hydrophobic amino acid substitution in the active site of human carbonic anhydrase II. Biochemistry. 2007; 42:3803–3813. [PubMed: 17330962]
12. Zheng JY, Avvaru BS, Tu C, McKenna R, Silverman DN. Role of Hydrophilic Residues in Proton Transfer during Catalysis by Human Carbonic Anhydrase II. Biochemistry. 2008; 47:12028–12036. [PubMed: 18942852]
13. Jackman JE, Merz KM Jr. Fierke CA. Disruption of the active site solvent network in carbonic anhydrase II decreases the efficiency of proton transfer. Biochemistry. 1996; 35:16421–16428. [PubMed: 8987973]
14. Cui Q, Karplus M. Is a “proton wire” concerted or stepwise? A model study of proton transfer in carbonic anhydrase. Journal of Physical Chemistry B. 2003; 107:1071–1078.
15. Maupin CM, Saunders MG, Thorpe IF, McKenna R, Silverman DN, Voth GA. Origins of enhanced proton transport in the Y7F mutant of human carbonic anhydrase II. Journal of the American Chemical Society. 2008; 130:11399–11408. [PubMed: 18671353]

16. Khalifah RG, Strader DJ, Bryant SH, Gibson SM. C-13 Nuclear Magnetic-Resonance Probe of Active-Site Ionizations in Human Carbonic-Anhydrase B. Biochemistry. 1977; 16:2241–2247. [PubMed: 16641]
17. Silverman DN. Carbonic anhydrase: oxygen-18 exchange catalyzed by an enzyme with rate-contributing proton-transfer steps. Methods Enzymol. 1982; 87:732–752. [PubMed: 6294458]
18. Simonsson I, Jonsson BH, Lindskog S. C-13 NMR study of carbon dioxide-bicarbonate exchange catalyzed by human carbonic anhydrase-C at chemical-equilibrium. European Journal of Biochemistry. 1979; 93:409–417. [PubMed: 34514]
19. McPherson, A. Preparation and Analysis of Protein Crystals. Wiley; New York: 1982.
20. Otwinowski Z, Minor W. Processing of X-ray Diffraction Data Collected in Oscillation Mode. Methods Enzymol. 1997; 276:307–326.
21. Adams PD, Afonine PV, Bunkoczi G, Chen VB, Davis IW, Echols N, Headd JJ, Hung LW, Kapral GJ, Grosse-Kunstleve RW, McCoy AJ, Moriarty NW, Oeffner R, Read RJ, Richardson DC, Richardson JS, Terwilliger TC, Zwart PH. PHENIX: a comprehensive Python-based system for macromolecular structure solution. Acta Crystallographica Section D-Biological Crystallography. 2010; 66:213–221.
22. Fisher Z, Hernandez Prada JA, Tu C, Duda D, Yoshioka C, An H, Govindasamy L, Silverman DN, McKenna R. Structural and kinetic characterization of active-site histidine as a proton shuttle in catalysis by human carbonic anhydrase II. Biochemistry. 2005; 44:1097–1105. [PubMed: 15667203]
23. Tu CK, Silverman DN, Forsman C, Jonsson BH, Lindskog S. Role of histidine 64 in the catalytic mechanism of human carbonic anhydrase II studied with a site-specific mutant. Biochemistry. 1989; 28:7913–7918. [PubMed: 2514797]
24. An H, Tu C, Duda D, Montanez-Clemente I, Math K, Laipis PJ, McKenna R, Silverman DN. Chemical rescue in catalysis by human carbonic anhydrases II and III. Biochemistry. 2002; 41:3235–3242. [PubMed: 11863462]
25. Silverman DN, Tu C, Chen X, Tanhauser SM, Kresge AJ, Laipis PJ. Rate-equilibria relationships in intramolecular proton transfer in human carbonic anhydrase III. Biochemistry. 1993; 32:10757–10762. [PubMed: 8399223]
26. Mildvan AS, Weber DJ, Kuliopulos A. Quantitative Interpretations of Double Mutations of Enzymes. Archives of Biochemistry and Biophysics. 1992; 294:327–340. [PubMed: 1567189]
27. Mikulski RL, Silverman DN. Proton transfer in catalysis and the role of proton shuttles in carbonic anhydrase. Biochimica Et Biophysica Acta-Proteins and Proteomics. 2010; 1804:422–426.
28. Krebs JF, Fierke CA, Alexander RS, Christianson DW. Conformational Mobility of His-64 in the Thr200Ser Mutant of Human Carbonic Anhydrase-II. Biochemistry. 1991; 30:9153–9160. [PubMed: 1909891]
29. Riccardi D, Konig P, Guo H, Cui Q. Proton transfer in carbonic anhydrase is controlled by electrostatics rather than the orientation of the acceptor. Biochemistry. 2008; 47:2369–2378. [PubMed: 18247480]
30. Shimahara H, Yoshida T, Shibata Y, Shimizu M, Kyogoku Y, Sakiyama F, Nakazawa T, Tate S, Ohki SY, Kato T, Moriyama H, Kishida K, Tano Y, Ohkubo T, Kobayashi Y. Tautomerism of histidine 64 associated with proton transfer in catalysis of carbonic anhydrase. J Biol Chem. 2007; 282:9646–9656. [PubMed: 17202139]
31. Maupin CM, McKenna R, Silverman DN, Voth GA. Elucidation of the Proton Transport Mechanism in Human Carbonic Anhydrase II. Journal of the American Chemical Society. 2009; 131:7598–7608. [PubMed: 19438233]
32. Domsic JF, Williams W, Fisher SZ, Tu C, Agbandje-McKenna M, Silverman DN, McKenna R. Structural and Kinetic Study of the Extended Active Site for Proton Transfer in Human Carbonic Anhydrase II. Biochemistry. 2010; 49:6394–6399. [PubMed: 20578724]
33. Wu Y, Voth GA. A computer simulation study of the hydrated proton in a synthetic proton channel. Biophys J. 2003; 85:864–875. [PubMed: 12885634]
34. Roy A, Taraphder S. Role of protein motions on proton transfer pathways in human carbonic anhydrase II. Biochimica Et Biophysica Acta-Proteins and Proteomics. 2010; 1804:352–361.

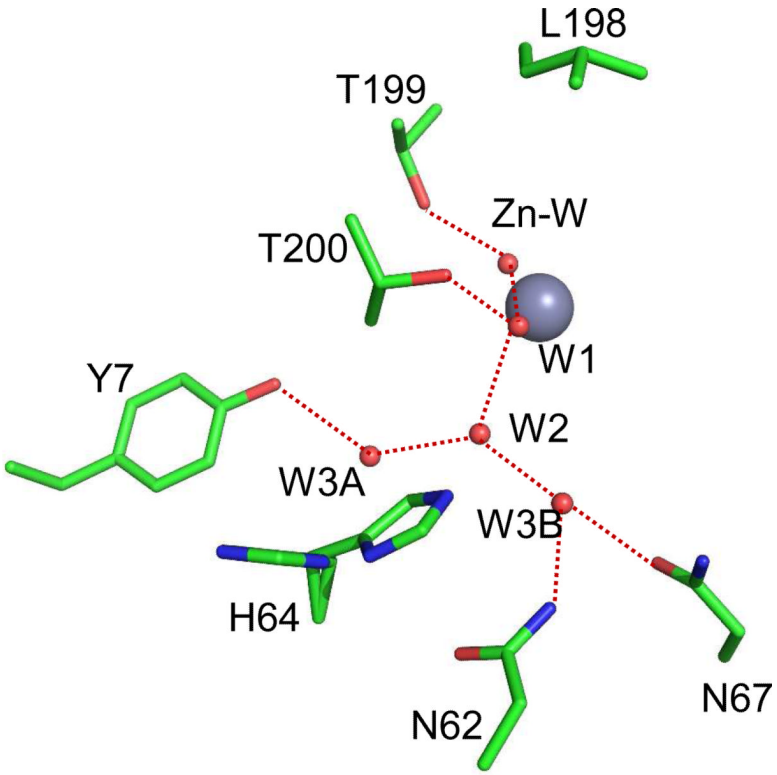

Figure 1.
Active site of wild type HCA II from the crystal structure at pH 8.0 (PDB code 2ili (8). The zinc ion and the oxygen of water molecules are shown as gray and red spheres, respectively. The water network of the active-site is labeled W1, W2, etc. Dashed red lines are assumed hydrogen bonds. The side chain of the proton shuttle His64 is shown in both the inward and outward orientations. This figure was generated and rendered with PyMOL (www.pymol.org).

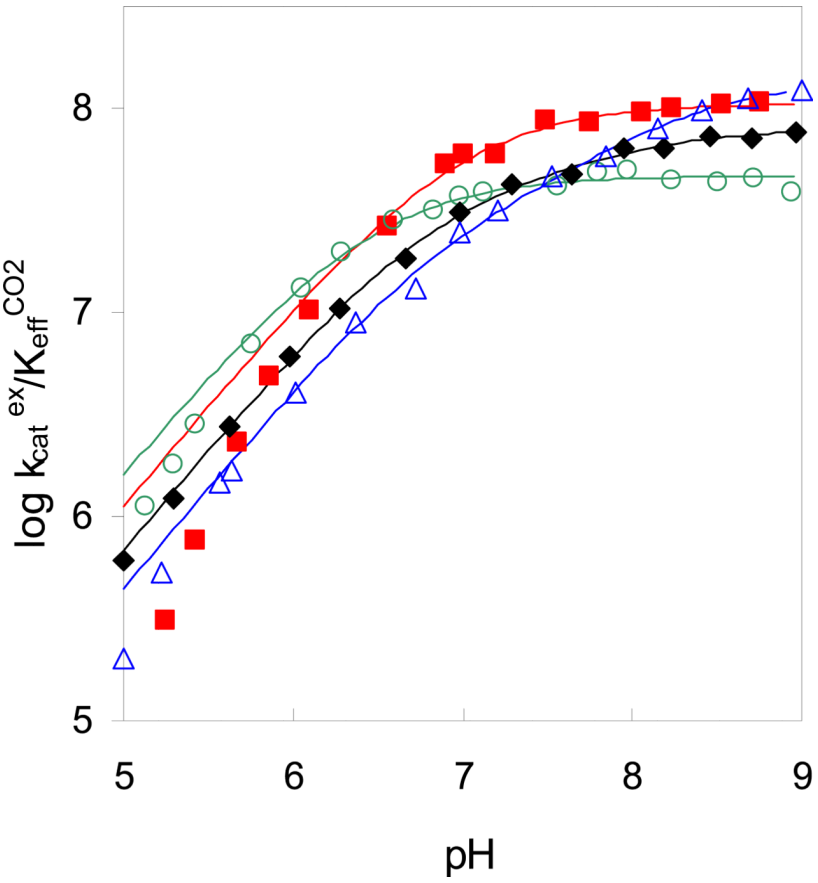

Figure 2.

The pH profiles for $k_{cat}^{ex}/K_{eff}^{CO2}$ ($M^{-1}s^{-1}$) for the hydration of CO_2 catalyzed by (◆) wild-type HCA II; (○) N67Q HCA II; (Δ) Y7F HCA II; and (■) Y7F-N67Q HCA II. Data were obtained by ^{18}O exchange between CO_2 and water using solutions containing 25 mM of all species of CO_2 and sufficient Na_2SO_4 to maintain 0.2 M ionic strength.

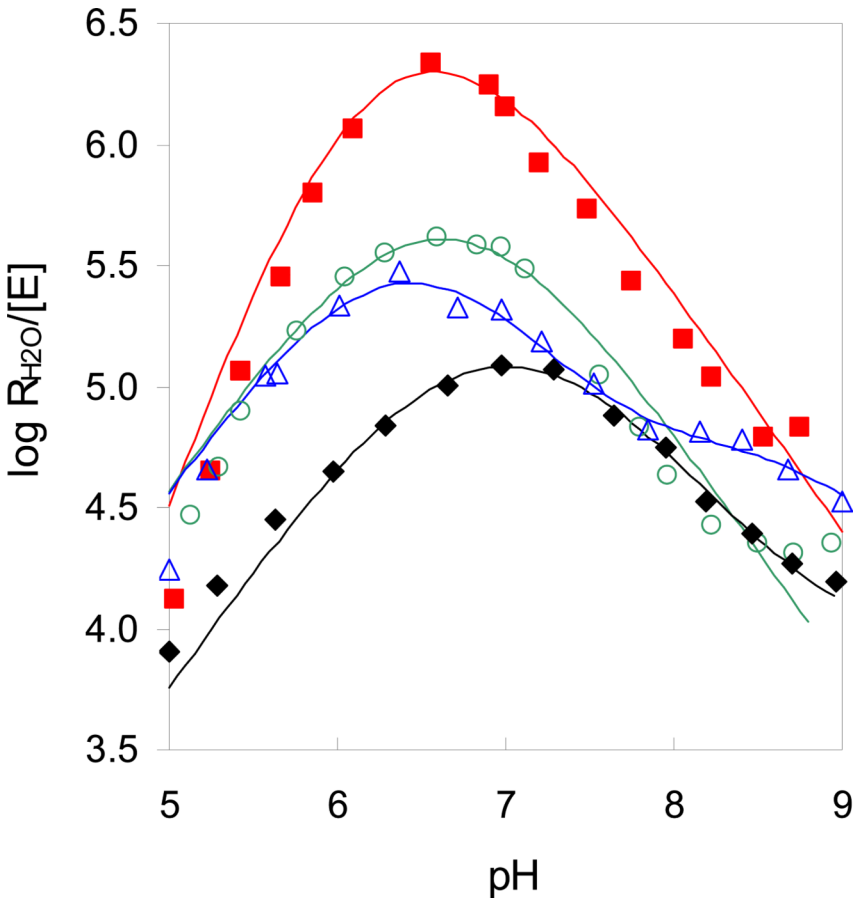

Figure 3.

The pH profiles for R_{H2O}/[E] (s^{-1}) the proton-transfer dependent rate of release of ^{18}O-labeled water catalyzed by (◆) wild-type HCA II; (○) N67Q HCA II; (Δ) Y7F HCA II; and (■) Y7F-N67Q HCA II. Conditions were as described in Figure 2.

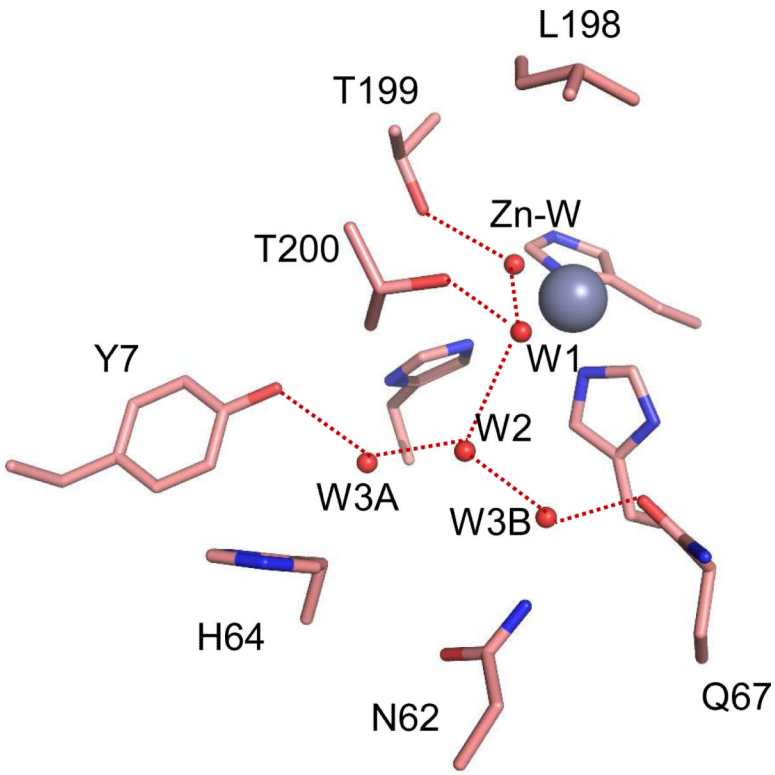

Figure 4.
The active-site structure for N67Q HCA II crystallized at pH 8.0. The three histidine residues (His94, His96, His119) coordinating the zinc (gray sphere) are not labeled. The oxygen atoms of water molecules identified in the active-site cavity are shown as red spheres and labeled W1, W2 .... Presumed hydrogen bonds are represented as dashed red lines. This figure was generated and rendered using Pymol.

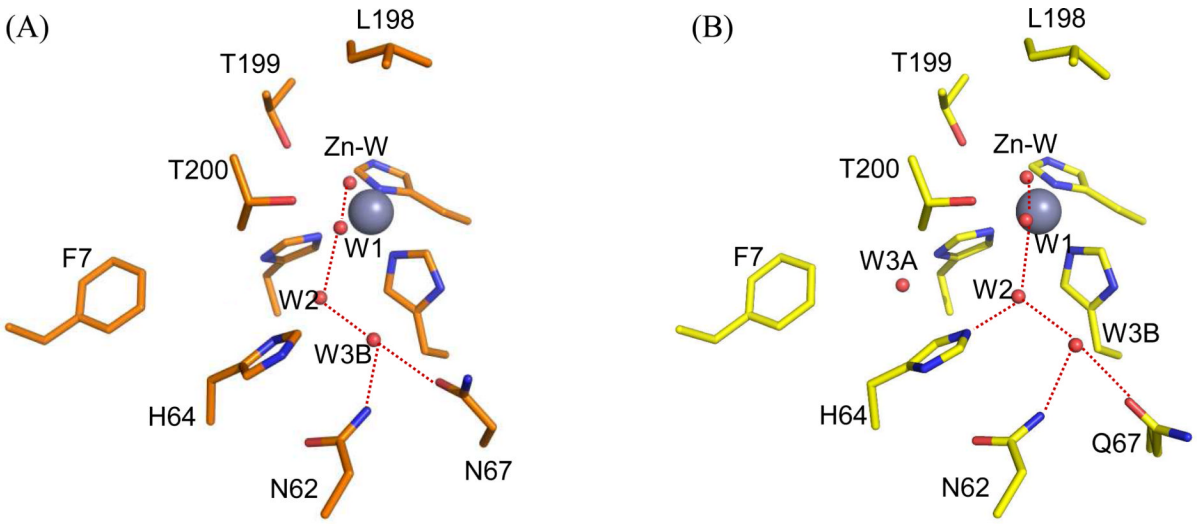

Figure 5.
Comparison of active-site structures for variants of HCA II crystallized at pH 8.0. (*A*) Y7F HCA II (PDB code 2nxt, (11)); and (*B*) Y7F-N67Q HCA II. This diagram was constructed as described as in Figure 4.

Table 1

Crystal Structure Data and Refinement Statistics for N67Q and Y7F+N67Q HCA II

Data-collection statistics	N67Q	Y7F-N67Q
Wavelength (Å)	1.5418	1.5418
Space group	P 2_1	P 2_1
Unit-cell parameters (Å,°) *a, b*, c (Å); β (°)	42.0, 41.2, 72.1; 104.3	42.1, 41.2, 71.9; 104.5
Total number of reflections	35820	31729
Redundancy	3.6 (2.5)*	3.8(3.6)
Completion %	97.7 (80.5)	99.7 (99.8)
Resolution (Å)	50.0-1.50 (1.55-1.50)	50.0-1.60 (1.66-1.60)
$^a R_{sym}$	7.3 (38.9)	8.4 (47.3)
I/σ(I)	14.5 (4.1)	13.1 (2.8)
$^b R_{cryst}$ (%)	18.5	16.6
$^c R_{free}$(%)	21.4	20.5
Amino acid residues	3-261	3-261
No. of protein atoms	2180	2199
No. of H_2O molecules	376	319
R.m.s.d. for bond lengths (Å), angles (°)	0.006 1.086	0.006 1.019
Ramachandran statistics (%) Most favored, allowed, outlier	87.6, 12.4, 0.0	86.6, 13.4, 0.0
Average B factors (Å^2) main-, side-chain, Zn, solvent	18.2, 21.4, 11.5, 29.6	19.8, 22.0, 10.5, 28.7

$^a R_{sym} = \Sigma |I - \langle I \rangle| / \Sigma \langle I \rangle$.

$^b R_{cryst} = (\Sigma ||F_o| - |F_c|| / \Sigma |F_{obs}|) \times 100$.

$^c R_{free}$ is calculated in same manner as $^b R_{cryst}$, except that it uses 5% of the reflection data omitted from refinement.

*Values in parenthesis represent highest resolution bin.

Table 2

Maximal Values of Rate Constants for Hydration of CO_2 and Proton Transfer in Dehydration Catalyzed by HCA II and Variants.

Enzyme	$k_{cat}^{exch}/K_{eff}^{CO2}$ CO_2 hydration ($\mu M^{-1}s^{-1}$)[a]	k_B proton transfer (μs^{-1})[b]
Wild type	120	0.80
Y7F[c]	120	3.9
N67Q	50	1.7
Y7F-N67Q[d]	80	9.0

[a] Measured from the exchange of ^{18}O between CO_2 and water in the hydration direction (eq 5). Derived for each variant by a fit of the data (as in Figure 2) to a single ionization. The standard errors for these rate constants are generally 15% or less.

[b] Measured from the exchange of ^{18}O between CO_2 and water (as in Figure 3) using eq 6 in the dehydration direction. The standard errors are 22% or less.

[c] Data at 10°C from Fisher et al. (11).

[d] Data at 10°C.

Table 3

Values of Apparent pK_a Obtained by Kinetic Measurements of Catalysis by HCA II and Variants

Enzyme	$pK_{a\ ZnH2O}$ [a]	$pK_{a\ ZnH2O}$ [b]	$pK_{a\ His64}$ [b]
wild type	6.9	6.8	7.2
Y7F[c]	7.1	7.0	6.0
N67Q	6.5	6.7	6.6
Y7F-N67Q[d]	6.9	6.3	6.2

[a] Measured from a fit of the data of Figure 2 to a single ionization. The standard errors in pK_a are mostly ± 0.1 and no greater than ± 0.2.

[b] Measured from the fits of eq 6 to the data of Figure 3. The values of pK_a have standard errors no greater than ± 0.2.

[c] These data at 10 °C from Fisher et al. (11).

[d] These data at 10 °C.

Table 4

Comparison of Distances (Å) in the Proposed Hydrogen Bond Network Determined from the Crystal Structures of Variants of HCA II.

	WT	Y7F[a]	Y7F-N67Q	N67Q
ZnSolvent-W1	2.7	2.7	2.7	2.7
W1-W2	2.7	2.6	2.6	2.9
W2-W3A	2.8	n/a	4.3	2.9
W2-W3B	2.7	2.6	3.1	2.4
W2-H64(N^{δ})	3.2/6.3	3.2	2.9	6.7
ZnSolvent-H64(N^{δ})	7.2/10.0	7.1	6.7	10.5
H64	in/out	In	in	out

[a]These data from (11)